Journal of Petroleum Science and Engineering 165 (2018) 616–626

Contents lists available at ScienceDirect

Journal of Petroleum Science and Engineering

journal homepage: www.elsevier.com/locate/petrol

Controls of natural fractures on the texture of hydraulic fractures in rock

Xianyu Zhao [a], Tao Wang [a,*], Derek Elsworth [b], Yunlong He [a], Wei Zhou [a], Li Zhuang [c], Jun Zeng [d], Suifeng Wang [e]

[a] State Key Laboratory of Water Resources and Hydropower Engineering Science, Wuhan University, Wuhan, China
[b] Department of Energy and Mineral Engineering, G3 Center and EMS Energy Institute, Penn State University, University Park, PA, USA
[c] Korea Institute of Civil Engineering and Building Technology, Goyang, Gyeonggi, Republic of Korea
[d] Sichuan Water Resources and Hydroelectric Investigation & Design Institute, Chengdu, China
[e] Engineering Faculty, China University of Geoscience, Wuhan, China

ARTICLE INFO

Keywords:
Hydraulic fracturing
Jointed rock mass
DEM
Crack propagation

ABSTRACT

Hydraulic fracturing plays an important role in the exploitation of oil, shale gas and coal seam gas resources – all of which contain natural fractures. We systematically explore the role of the pre-existing texture of such natural fractures on the form of the resulting stimulated reservoir volume (SRV). A blocky discrete element model (DEM) coupled with fluid flow is used to explore this response. Numerical predictions for the evolution of fluid pressure and fracture width at the well are compared with first-order analytical approximations of the zero-toughness solution (FMO). We then construct four typical joint system models separately comprising orthogonal, staggered, diagonal and randomly oriented joints and conduct the virtual hydraulic fracturing simulations via DEM. This defines the influence of structure on breakdown pressure and fracture propagation and allows the analysis of the main factors that influence behavior and resulting SRV. Results for the four forms of jointed rock mass show that: (1) the aggregate/mean extension direction of the fractures is always along the direction of the maximum principal stress but significant deviations may result from the pre-existing fractures; (2) there are negative correlations between the maximum fracture aperture with both Poisson ratio and elastic modulus, but the breakdown pressure is only weakly correlated with Poisson ratio and elastic modulus; (3) an increase in injection rate results in a broader fracture process zone extending orthogonal to the principal fracture, and the breakdown pressure and interior fracture aperture also increase; (4) an increase in fluid viscosity makes the fractures more difficult to extend, and the breakdown pressure and interior fracture aperture both increase accordingly.

1. Introduction

Hydraulic fracturing (HF) is widely used as a method for enhancing oil and gas production and in increasing recoverable reserves. Introduced in 1949, hydraulic fracturing has evolved into a standard operating practice, with many treatments completed (Veatch, 1983). Today, HF is used extensively in the petroleum industry to stimulate oil and gas wells to increase their productivity (Adachi et al.,2007; Yuan et al., 2017a,b; Yuan et al., 2018).

During the past few decades, considerable effort has been applied to understand the mechanics of hydraulic fracturing through numerical methods. The Finite Element Method (FEM) and the Boundary Element Method (BEM) have each been used to simulate HFs in complex formations (Papanastasiou, 1997; Vychytil and Horii, 1998). These have included three-dimensional nonlinear fluid-mechanics coupling of FEM to represent staged fracturing processes of a horizontal well in the Daqing Oilfield (Zhang et al., 2010). Coupling algorithms combining FEM and meshless methods have been applied for the simulation of the dynamic propagation of fracturing under either external forces or hydraulic pressure (Wang et al., 2010). In attempts to validate the models, microseismic monitoring has been used to image the extent and nature of hydraulic fractures. One of the major findings of these studies is that the nature of the hydraulic fractures determined by observing the recorded seismicity does not generally agree with that predicted by conventional analytical and numerical models (Al-Busaidi et al., 2005). For this reason, discontinuum-based Distinct Element Methods (DEM) have been applied to the simulation of HF. With these techniques, the continuum is divided into distinct blocks or particles between which fluid can flow. This allows a better representation of hydraulic fracture growth in the rock mass, which may contain multiple pre-existing cracks, joints or flaws.

* Corresponding author.
E-mail address: htwang@whu.edu.cn (T. Wang).

https://doi.org/10.1016/j.petrol.2018.02.047
Received 29 November 2017; Received in revised form 8 February 2018; Accepted 19 February 2018

DEM has been used to investigate the mechanics of naturally fractured reservoirs subject to a constant rate of fluid injection (Harper and Last, 1990). Moreover, Granular mechanics implementations of DEM have become an effective tool for modeling crack propagation (Potyondy and Cundall, 2004). This method provides a way to simulate the process of crack formation and extension in rock masses when injecting fluid into the borehole, with the simulation results compared to acoustic emission data from experiments (Al-Busaidi et al., 2005). The fluid viscosity and selected particle size distribution exert significant influence on simulations of HF in competent rock when using coupled flow-deformation DEM codes (Shimizu, 2010; Shimizu et al., 2011). An attempt has been made to validate the several proposed methods for shut-in pressure, under various remote stress regimes and various rock properties using DEM (Choi, 2012). PFC^{2D} was used to simulate HF propagation within a coal seam (Wang et al., 2014). The objectives of this study is to investigate mechanisms governing HF propagation in coal seams, propose schemes that may achieve the desired fracturing effects and aid in optimally guiding engineering practice.

Primarily from mine-back experiments and laboratory tests, geologic discontinuities such as joints, faults, and bedding planes are observed to significantly affect the overall geometry of the resulting hydraulic fractures (Warpinski and Teufel, 1987). This can occur by arresting the growth of the fracture, increasing fluid leak off, hindering proppant transport, and in enhancing the creation of multiple fractures. Discrete fracture network (DFN) modeling is an approach for representing and assessing complex fracture growth and associated production prediction through generated fractures coupling with DEM (McLennan et al., 2010; Riahi and Damjanac, 2013). A microscopic numerical system has been used to model the interaction between HFs and natural fractures (Han et al., 2012). Preliminary results obtained using combined finite-discrete element techniques have also been used to study the interaction between fluid driven fractures and natural rock mass discontinuities (Grasselli et al., 2015). *HF Simulator* (A DEM solution based on a quasi-random lattice of nodes and springs) has been used to represent hydraulic fracturing in jointed rock masses (Damjanac and Cundall, 2016). The effect of natural existing fractures on fluid-driven hydraulic fracture growth is investigated by analyzing the variation of fracture radius, cumulative crack number, and growth rate of porosity versus injection time based on PFC^{2D} (Wang et al., 2017).

In this paper, we use a DEM code (UDEC) to simulate and analyze the characteristics of HF propagation in complex jointed rock masses to codify crack propagation influences of natural fractures. After verification of the first order approximation of the zero-toughness solution of HF, correlations among the initial stress, injection parameters and the performance of fractures induced by HF in naturally fractured media are then all studied.

2. Simulation mechanism of UDEC

It is well known that accommodating the role of discontinuities in rock masses is a challenging task. UDEC is specifically developed to model discontinuous problems. It can accommodate many discontinuities and permits the modelling system to undergo large geometrical change through the use of a contact updating scheme (Fig. 1). In UDEC, the deformation of a fractured rock mass consists of the elastic/plastic deformation of blocks of intact rock, together with the displacements along and across fractures. The motion of a block is characterized by Newton's second law of motion, expressed in central finite difference form with respect to time. Calculations are performed over one timestep in an explicit time-marching algorithm. For deformable blocks, numerical integration of the differential equation of motion is used to determine the incremental displacements at the gridpoints of the triangular constant strain element within the blocks. The incremental displacements are then used to calculate the new stresses within the element through an appropriate constitutive equation (Itasca, 2015).

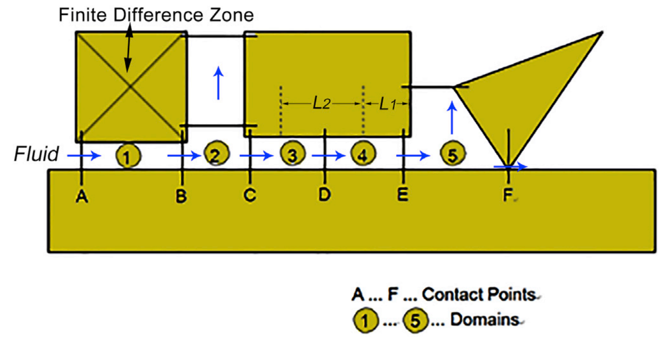

Fig. 1. Contacts, domains and flow between domains between blocks. Modified from Lemos and Lorig (1990).

2.1. Joint behavior model

The data structure only needs two types of contacts to represent a system of blocks: corner-to-corner contacts and edge-to-corner contacts. These are termed “numerical contacts.” Physically, however, edge-to-edge contact is important, because it corresponds to the case of a rock joint closed along its entire length. A physical edge-to-edge contact corresponds to a domain with exactly two numerical contacts in its linked-list. The joint is assumed to extend between the two contacts and to be divided in half, with each half-length supporting its own contact stress. Incremental normal and shear displacements are calculated for each point contact and associated length (i.e., L_1 and L_2 in Fig. 1).

Many types of constitutive models for edge-to-edge contact may be contemplated. The basic joint model used in UDEC captures several of the features that are representative of the physical response of joints. In the normal direction, the incremental normal stress and the incremental normal displacement are $\Delta\sigma_n$ and Δu_n respectively, and the stress-displacement relation is assumed to be linear and governed by the stiffness k_n such that

$$\Delta\sigma_n = -k_n \Delta u_n. \tag{1}$$

A more comprehensive displacement-weakening model is also available in UDEC. This model (the continuously yielding joint model) is intended to simulate the intrinsic mechanism of progressive damage of the joint under shear.

There is also a limiting tensile strength $\tau_{\max}$ for the joint. If the tensile strength is exceeded (i.e., if $\sigma_n < -\tau_{\max}$), then $\sigma_n = 0$. Similarly, in shear, the response is controlled by a constant shear stiffness k_s. The shear stress τ_s is limited by a combination of cohesive (C) and frictional (ϕ) strength. Thus, if

$$|\tau_s| \le C + \sigma_n + \tan\phi = \tau_{\max} \tag{2}$$

then

$$\Delta\tau_s = -k_s \Delta u_s^e. \tag{3}$$

Or, if

$$|\tau_s| \ge \tau_{\max} \tag{4}$$

then

$$\tau_s = sign(\Delta u_s)\tau_{\max} \tag{5}$$

where, $\Delta\tau_s$ is the incremental shear stress; Δu_s^e is the elastic component of the incremental shear displacement; and Δu_s is the total incremental shear displacement.

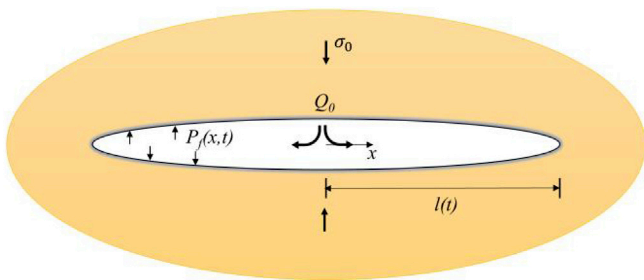

Fig. 2. Hydraulic fracture propagating in an impermeable elastic medium.

2.2. Fluid-mechanical coupling

A fully coupled mechanical-hydraulic analysis is performed, in which fracture conductivity is dependent on mechanical deformation and, conversely, joint fluid pressures affect the mechanical deformation. The numerical implementation for fluid flow makes use of the domain structure. For a closely packed system, there is a network of domains, each of which is assumed to be filled with fluid at uniform pressure and which communicates with its neighbors through contacts. Domains are separated by the contact points (designated by letters A to F in Fig. 1), which are the points at which the forces of mechanical interaction between blocks are applied. Because deformable blocks are discretized into a mesh of triangular elements, gridpoints may exist not only at the vertices of the block, but also along the edges. A contact point is placed wherever a gridpoint meets an edge or a gridpoint of another block. For example, in Fig. 1, contact D implies the existence of a gridpoint along one of the edges in contact. Consequently, the joint between the two blocks is represented by two domains: 3 and 4. If a finer internal mesh were adopted, the joint would be represented by a larger number of contiguous domains. Therefore, the degree of refinement of the numerical representation of the flow network is linked to the mechanical discretization adopted, and can be appropriately defined for different purposes.

Flow is governed by the pressure differential between adjacent domains. The flow rate is calculated in two different ways, depending on the type of contact. For a point contact (i.e., corner-edge, as contact F in Fig. 1, or corner-corner), the flow rate q from a domain with pressure p_1 to a domain with pressure p_2 is given by

$$q = -k_c \Delta p \tag{6}$$

where $k_c =$ a point contact permeability factor, and

$$\Delta p = p_2 - p_1 + \rho_w g (y_2 - y_1) \tag{7}$$

where ρ_w is the fluid density; g is the acceleration of gravity (assumed to act in the negative y-direction); and y_1, y_2 are the y-coordinates of the domain centers.

The hydraulic aperture is given, in general, by

$$a = a_0 + u_n \tag{8}$$

where a_0 is the joint aperture at zero normal stress; and u_n is the joint normal displacement.

A minimum value, a_{res}, is assumed for the aperture, below which mechanical closure does not affect the contact permeability. A maximum value, $a_{\max}$, is also assumed, for efficiency, in the explicit calculation (set to five times a_{res}).

3. Verification of hydraulic fracturing in UDEC

We first verify the validity of the code by performing a comparison with solutions for the propagation of an idealized fracture in a homogeneous porous medium. This is defined through comparisons of propagation history and width with time.

3.1. Zero-toughness solution (FMO)

A hydraulic fracture is a fluid-driven crack that advances as a viscous fluid is injected into a central borehole. This behavior may be reduced to two dimensions, as a plane strain problem. The Kristianovic-Geerstma-de Klerk (KGD) model represents behavior as shown in Fig. 2. A zero toughness solution exists when a viscous fluid is injected at a constant rate into a planar crack and zero strength at the tip is adopted (Adachi and Detournay, 2002).

The material parameters μ' and E' are defined as $\mu' = 12\mu, E' = E/(1-\nu^2)$, where μ is fluid viscosity, E and ν are rock Young modulus and Poisson ratio respectively. The fracture width w, fluid pressure p and the half fracture length $l(t)$ can be represented as (Adachi and Detournay, 2002):

$$w = \varepsilon(t) L(t) \Omega[\xi, P(t)], p = \varepsilon(t) E' \Pi[\xi, P(t)], l(t) = \gamma[P(t)] L(t) \tag{9}$$

and

$$\varepsilon(t) = \left(\frac{\mu'}{E't}\right)^{1/3}, L(t) = \left(\frac{E' Q_0^3 t^4}{\mu'}\right)^{1/6} \tag{10}$$

where Q_0 is the injection rate; $\xi = x/l(t)$ is scaled coordinate $(0 \le \xi \le 1)$; $\varepsilon(t)$ is small dimensionless parameter; $P(t)$ is dimensionless evolution parameter; and $\gamma[P(t)]$ is dimensionless fracture length.

The first order approximation $\overline{F}_{mo}^{(1)}$ of the zero toughness solution is

$$\overline{\Omega}_{mo}^{(1)} = A_0 (1-\xi^2)^{2/3} + A_1^{(1)} (1-\xi^2)^{5/3} + B^{(1)} \left[4\sqrt{1-\xi^2} + 2\xi^2 \ln\left| \frac{1-\sqrt{1-\xi^2}}{1+\sqrt{1-\xi^2}} \right| \right] \tag{11}$$

Table 1
Rock and Fluid properties for the simulations.

Model properties		Joint properties		Fluid properties	
Rock density ρ /kg·m^{-3}	2600	Joint aperture at zero normal stress a_0 /m	1.35e-5	Fluid viscosity μ /Pa·s	0.001
Young modulus E /GPa	40	Minimum aperture a_{ares} /m	8.5e-6	Fluid density ρ_w /kg·m^{-3}	1000
Poisson ratio ν	0.22	Joint stiffness k_n, k_s /GPa·m^{-1}	2000	Fluid modulus E_w /MPa	100
Vertical stress σ_{yy} /MPa	−10	Joint cohesion C /MPa	0		
Horizontal stress σ_{xx} /MPa	−15	Joint friction angle φ /°	45		
Injection rate Q_0 /m^2·s^{-1}	0.0017	Joint tension σ_t /MPa	−9		

$$\prod_{mo}^{(1)} = \frac{1}{3\pi} B\left(\frac{1}{2};\frac{2}{3}\right) A_{0\,2}F_1\left(-\frac{1}{6},1;\frac{1}{2};\xi^2\right) + \frac{10}{7} A_1^{(1)}\,{}_2F_1\left(-\frac{1}{6},1;\frac{1}{2};\xi^2\right) + B^{(1)}(2-\pi|\xi|) \tag{12}$$

where $A_0 = 3^{1/2}$,$A_1^{(1)} \simeq -0.156$, and $B^{(1)} \simeq 6.63 \times 10^{-2}$; B=Euler beta function, and ${}_2F_1$ = hypergeometric function. Thus, $\overline{\Omega}_{mo}^{(1)} \simeq 1.84$ and $\gamma_{mo}^{(1)} \simeq 0.616$.

3.2. UDEC model

In accordance with the zero toughness condition investigated, three conditions are applied in UDEC: 1) the saturation of the fracture is initially set to be zero, defining that the fracture is dry; 2) the joint offers no resistance to opening; and 3) the condition of zero flow ahead of the crack tip is enforced. The data used in this section are presented in Table 1.

The UDEC model domain used in this section is 10 m × 10 m, as shown in Fig. 3. The zone (block) size is uniform and equal to 0.078 m. The matrix is elastic, with a Young's modulus of 40 GPa and a Poisson ratio of 0.22. A through going joint is specified at mid-height in the model with an initial stress state, $\sigma_{yy} = -10$ MPa and $\sigma_{xx} = -15$ MPa, applied. Full fluid-mechanical coupling is applied.

The joint stiffness is related to the apparent stiffness of neighboring zones with 2000 GPa/m used here. The joint is assumed to have no resistance to opening, and thus the joint cohesion is set to be zero. To prevent premature fracturing during the transient phase experienced by the model as it reaches a quasi-static state, a high value of joint friction (45°) is initially assigned, with a residual value of zero. The initial value of joint tensile strength is chosen to be −9 MPa, which is a slightly smaller than the initial normal stress (−10 MPa) – this is to prevent fracture propagation along the entire joint; the residual value is zero. The minimum aperture a_{ares} of the joint is set to be $8.5 \cdot 10^{-6}$ m, and the aperture at zero normal stress a_0 is the sum of a_{ares} and the ratio of normal stress and the joint stiffness.

The fluid flow is assumed to be slightly compressible, with a bulk modulus of 100 MPa. It is much smaller than its real value and is scaled to accelerate the numerical computation. Fluid injection is at a constant rate

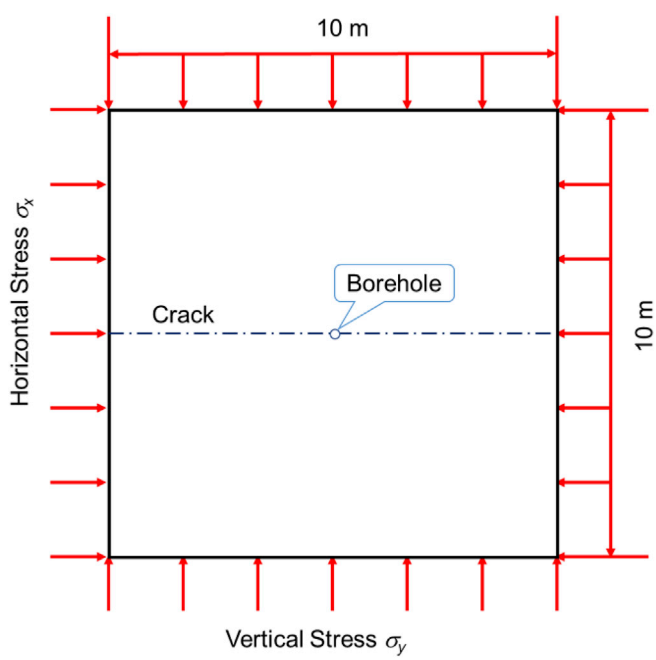

Fig. 3. Hydraulic fracturing in a model containing a prospective fracture at mid-height and with zero toughness.

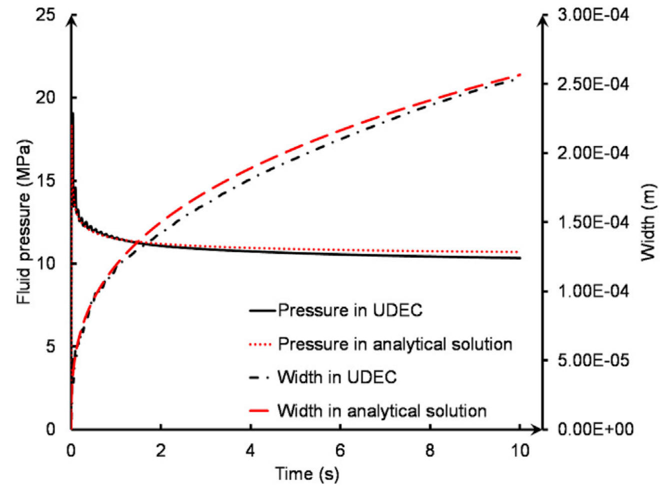

Fig. 4. Pressure and width at the well versus time for a KGD fracture of zero toughness.

(0.0017 m^2/s). It is specified for the well, located at the origin of axes (center of the model) with a fluid viscosity of 0.001 Pa s. The fluid-mechanical simulation is completed for a total of 10 s of injection in quasi-static mode.

3.3. Verification

Verification is completed for the propagation of a pressurized fracture with fluid pressure and fracture compared with the analytical FMO solutions. The fracture width is calculated from the hydraulic aperture, by subtracting the initial aperture a_{ares}.

The fluid pressure and width at the well are both shown versus time in Fig. 4. Fluid pressure and fracture width at the well predicted by UDEC satisfactorily match the FMO solution. As observed in Fig. 4, the UDEC solution for width at the well is slightly lower than the analytical solution.

The prediction of fracture pressure from UDEC is compared to the first order approximation of the zero toughness solution (Adachi and Detournay, 2002; Detournay, 2004) at 10 s after the initiation of fluid injection in Fig. 5(a). The UDEC pressure solution underestimates the value predicted by the analytical solution by only ~5%.

The UDEC prediction for fracture width is compared to the FMO solution at 10 s after fluid injection in Fig. 5(b). The fracture width predicted by UDEC in the reported simulations is underestimated, when compared to the FMO solution, by only ~3%. This correspondence between the UDEC prediction and the FMO solution are overall excellent.

4. Numerical simulation of HF in jointed rock mass

We now apply UDEC to explore the evolution of HFs in jointed rock masses. Four types of natural fracture distributions are used to simulate HF propagation in rock masses under the same conditions. Breakdown pressures and maximum fracture opening in these four cases are shown in this section.

4.1. Establishment of different jointed rock mass models

The size of the overall model is 10 m × 10 m. The model is square (Fig. 6) with loads on the four boundaries applied by a servo mechanism to adjust the position and speed of the walls and to retain the in situ stresses constant. A vertical principal stress is applied to the upper and lower walls and a horizontal principal stress is applied to the left and right walls. Four models are constructed as shown in Fig. 6. All the rock blocks in the model are of isotropic elastic material, and the joints in all

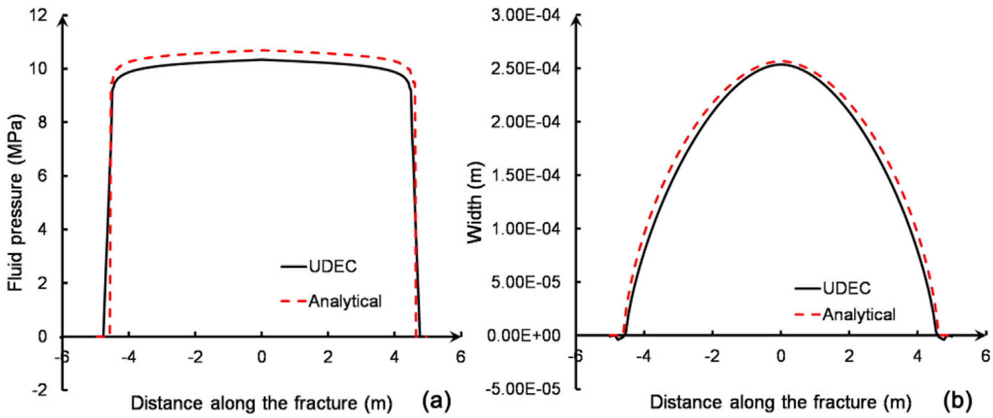

Fig. 5. (a) Pressure and (b) width distribution in the fracture after 10 s of injection.

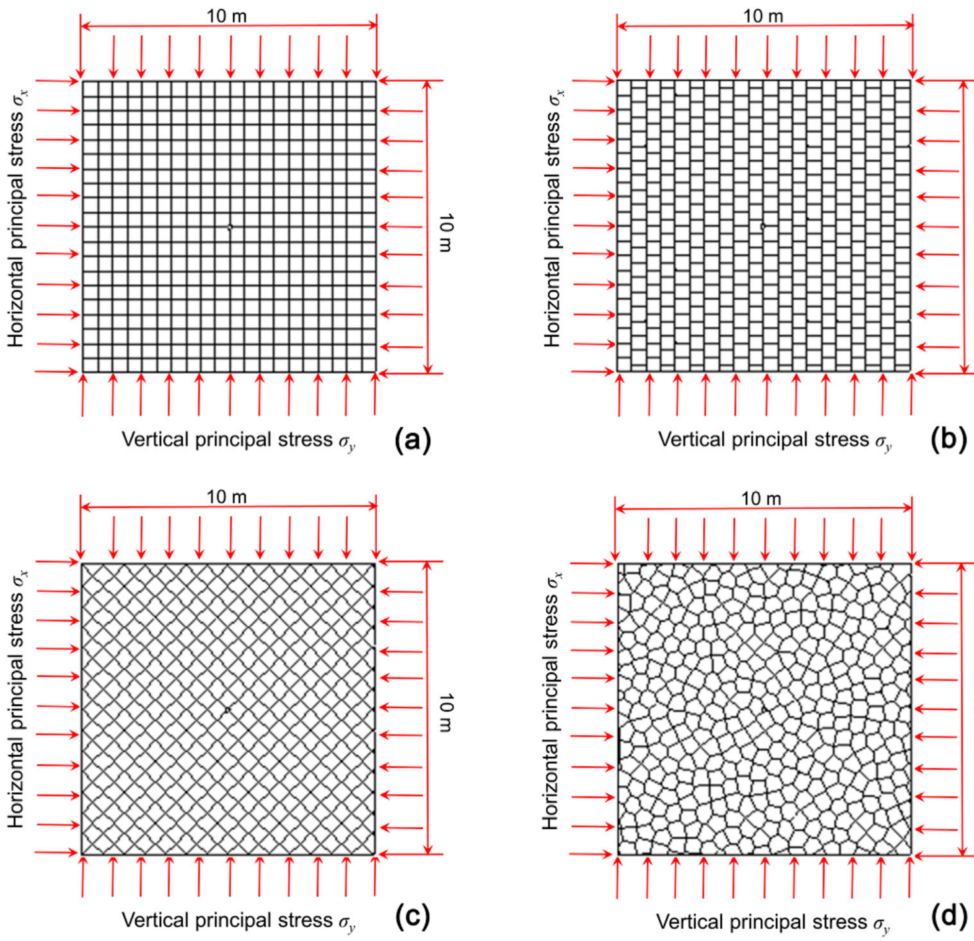

Fig. 6. Schematic diagram of HF model of rock masses: (a) orthogonal jointed rock mass; (b) staggered jointed rock mass; (c) diagonal jointed rock mass; (d) random jointed rock mass.

Table 2
Micro-mechanical and macro-mechanical parameters of the model.

Block model		Joint model	
Young modulus E /GPa	4	Normal stiffness k_n /GPa·m^{-1}	70
Density ρ /kg·m^{-3}	2600	Shear stiffness k_s /GPa·m^{-1}	70
Poisson ratio ν	0.22	Internal friction angle φ /°	45
		Cohesion C /MPa	30
		Tensile strength σ_t /MPa	14
		a_{res} /m	2.0e-5
		a_0 /m	6.8e-5

Table 3
In-situ stress and water injection parameters.

Parameter	numerical value
Vertical principal stress σ_y /MPa	10
Horizontal principal stress σ_x /MPa	15
Duration of injecting water t /s	10
Injection rate Q_0 /m^2·s^{-1}	4.0e-4
Fluid viscosity μ /Pa·s	0.001
Initial pore pressure /MPa	0

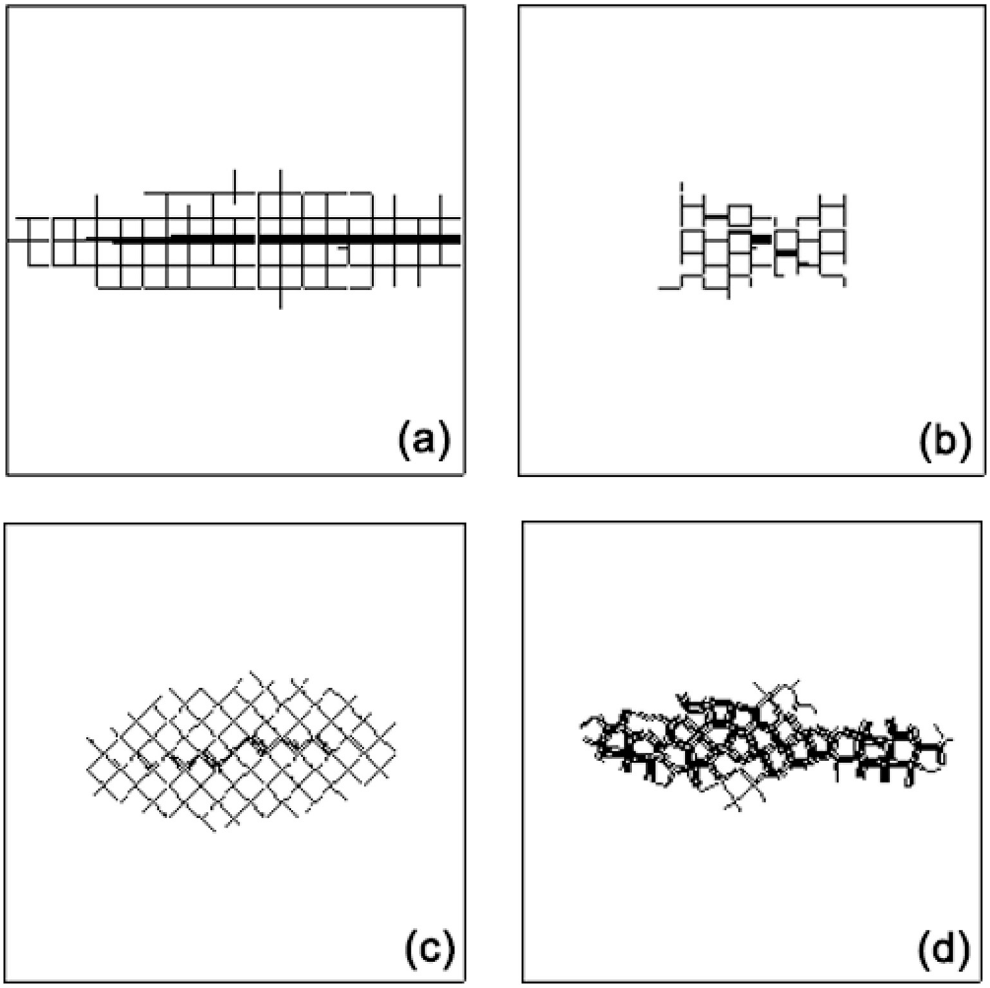

Fig. 7. Textures of fracture propagation in different jointed rock masses (t = 10s): (a) orthogonal jointed rock mass; (b) staggered jointed rock: (c) diagonal jointed rock mass; (d) random jointed rock mass.

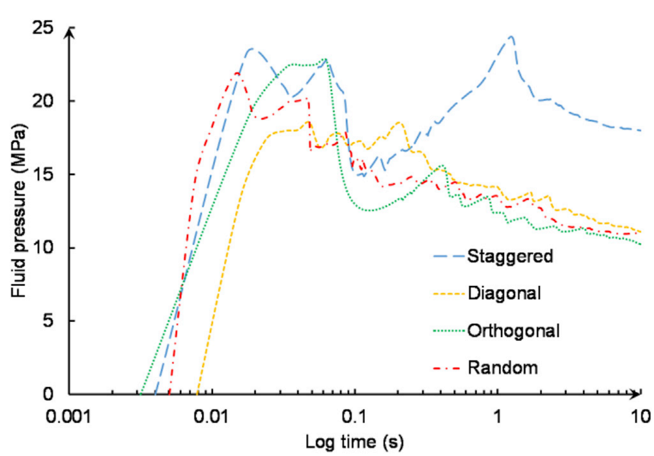

Fig. 8. Pore pressure with time for jointed rock masses: (a) diagonal; (b) staggered; (c) orthogonal; (d) random.

the models exhibit the characteristics of Coulomb sliding with residual strength.

4.2. Parameters in HF

During HF simulation a point source is applied at the center of the model to represent the injection borehole (as shown in Fig. 6). The initial pore pressure is 0 MPa and subsequently water is continuously injected into the hole at a constant flow rate until the fracture develops and propagates. The micro- and macro-scopic parameters of the rock mass and the in-situ stress and water injection parameters of the model are shown in Tables 2 and 3, respectively.

Table 4
Breakdown pressure and maximum crack opening for different jointed rock masses.

Type of jointed rock mass	Breakdown pressure P_b/MPa	Maximum crack opening W/m
Orthogonal jointed rock mass	22.74	3.739×10^{-4}
Staggered jointed rock mass	23.17	1.319×10^{-3}
Diagonal jointed rock mass	18.56	4.071×10^{-4}
Random jointed rock mass	21.92	6.271×10^{-4}

4.3. Numerical simulation results of HF

For the four jointed rock mass models described in this paper (Fig. 6), the spacing between joints is 0.5 m. The spatial distribution of hydraulic fractures in the jointed rock masses and the fluid penetration are shown in Fig. 7, and the changes of injection pressures with time are shown in Fig. 8. In this, the thin lines indicate where the fluid has permeated into the corresponding joints and the thick line(s) indicate(s) the HF fractures caused by the water injection.

Table 5
Cases of different in-situ stress conditions considered in the models.

Case	σ_y /MPa	σ_x /MPa	K
1	10	5	0.5
2	10	8	0.8
3	10	10	1
4	10	15	1.5
5	10	20	2
6	8	16	2
7	12	24	2
8	14	28	2

Apparent from Fig. 7 is that the distribution of fractures in structurally different jointed rock masses impacts the extension of the hydraulic fracture extent – causing propagation not always along the direction of maximum principal stress. For example, the crack distribution in the staggered jointed rock mass is relatively uniform in both directions - the staggered joints prevent the fracture from extending along the direction of maximum principal stress (horizontal in figure). The random jointed rock mass has multiple natural fractures, which are more favorable to the penetration of fluid in their channels. The pressure-time history curves shown in Fig. 8 define the changing fluid pressure during HF. Each curve initially rises sharply since the injection rate is larger than the diffusion rate of fluid into the rock mass. However, once the rock mass ruptures and the fluid flows along the newly-created cracks, the pressure in the hole peaks, and then drops. Unlike the other curves shown in Fig. 8, a second peak can be seen in the case of the staggered jointed rock mass at t = 2 s. This is because the structure of the staggered joints is segmented, and the flow channel for fluid is blocked by the discontinuous joints.

Breakdown pressures and maximum crack opening displacements in the four simulation examples are listed in Table 4. From Table 4 it is apparent that: under the same conditions in all simulation experiments, the breakdown pressure for the diagonally jointed rock mass is the smallest, and the breakdown pressure for the staggered joint set is the largest.

5. Factors controlling HF in jointed rock masses

There are various instances where viscous fluid drives growth of a fracture near a free surface (Wang and Detournay, 2018). HF is used to rupture the rock masses and to increase the permeability and reduce the pressure diffusion length from the interior of the reservoir to the conductive fracture. The resulting fractures from HF affect the permeability of the rock mass, and the changes in fluid pressure further modify the stress field – further influencing propagation, especially where heterogeneities exist. This process is readily influenced by many factors, including the mechanical properties of the rock mass, in situ stress conditions, the characteristics of the fracturing fluid, and the structure of the rock mass. The influence of reservoir elastic modulus and in-situ stress on the vertical propagation of HFs is explored by establishing a pseudo-three-dimensional model of the HF (Settari and Cleary, 1986). This shows that the vertical propagation is strongly sensitive to elastic modulus and confining stress. The effects of several parameters (in-situ stress contrast, modulus contrast, tensile strength contrast and viscosity of the fracturing fluid) on resulting fracture characteristics have also been

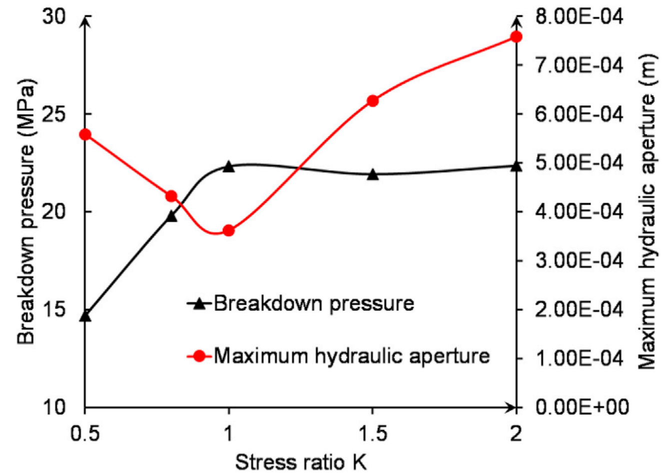

Fig. 10. Effect of stress ratio on breakdown pressure and maximum crack opening.

studied with a coupled FEM model (Zhang et al., 2010).

In the following we explore the impacts of in situ stress, injection rates and fluid viscosity on the form of fracturing developed in variously naturally fractured rock masses.

5.1. In situ stress conditions

The distribution of in-situ stress defines the initiation pressure, the direction of extension of the fracture and its evolving length. Two aspects are considered in this work to study the effect of in-situ stress conditions. These are the stress ratio and the stress magnitude. The size of the model, the meso-mechanical parameters of the contact model and injection parameters of the HF are shown in Tables 2 and 3, as used previously. The lateral and vertical boundary conditions are applied stresses σ_x and σ_y respectively, and these have the relationship that $\sigma_x = K \cdot \sigma_y$, where K is the stress ratio. Table 5 shows the calculation cases. Cases 1–5 are used to study the effect of stress ratio with the remainder used to study the effect of stress magnitude.

5.1.1. Stress ratio

Cases 1–5 (Table 5) have fixed magnitude of σ_y, but stress ratios K that transit from 0.5 to 2.0. Fig. 9 shows that the propagation direction changes as the stress ratio is modified – effectively changing the direction of the maximum principal stress. When $K < 1$, the fractures propagate continuously in the vertical direction. When $K = 1$, the propagation direction is at 45° to the horizontal. When $K > 1$, there is an obvious change in the propagation direction, that switches to along the horizontal direction. Hence, the propagation direction of hydraulic fractures is always parallel to the direction of maximum principal stress. It can also be seen from Fig. 9, that with an increase in the stress ratio K, the range of the fracture propagation (size of the stimulated region) is smaller.

Fig. 10 shows the effect of in-situ stress ratio on the maximum crack opening and the breakdown pressure. When the stress ratio $K < 1$, the maximum crack opening decreases and the breakdown pressure increases with an increase of K. When the stress ratio $K \geq 1$, the maximum

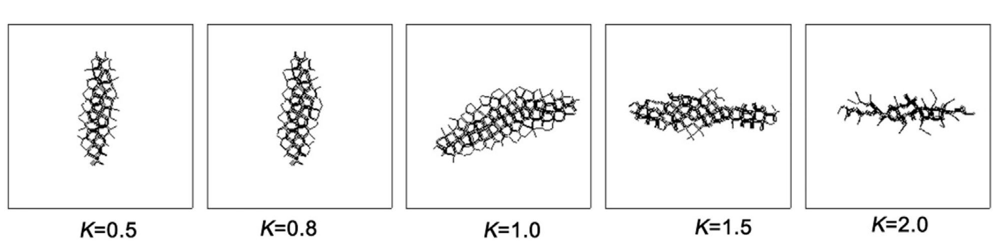

Fig. 9. Distribution of fractures in rock masses with randomly oriented joints under different stress ratio conditions ($t = 10$ s).

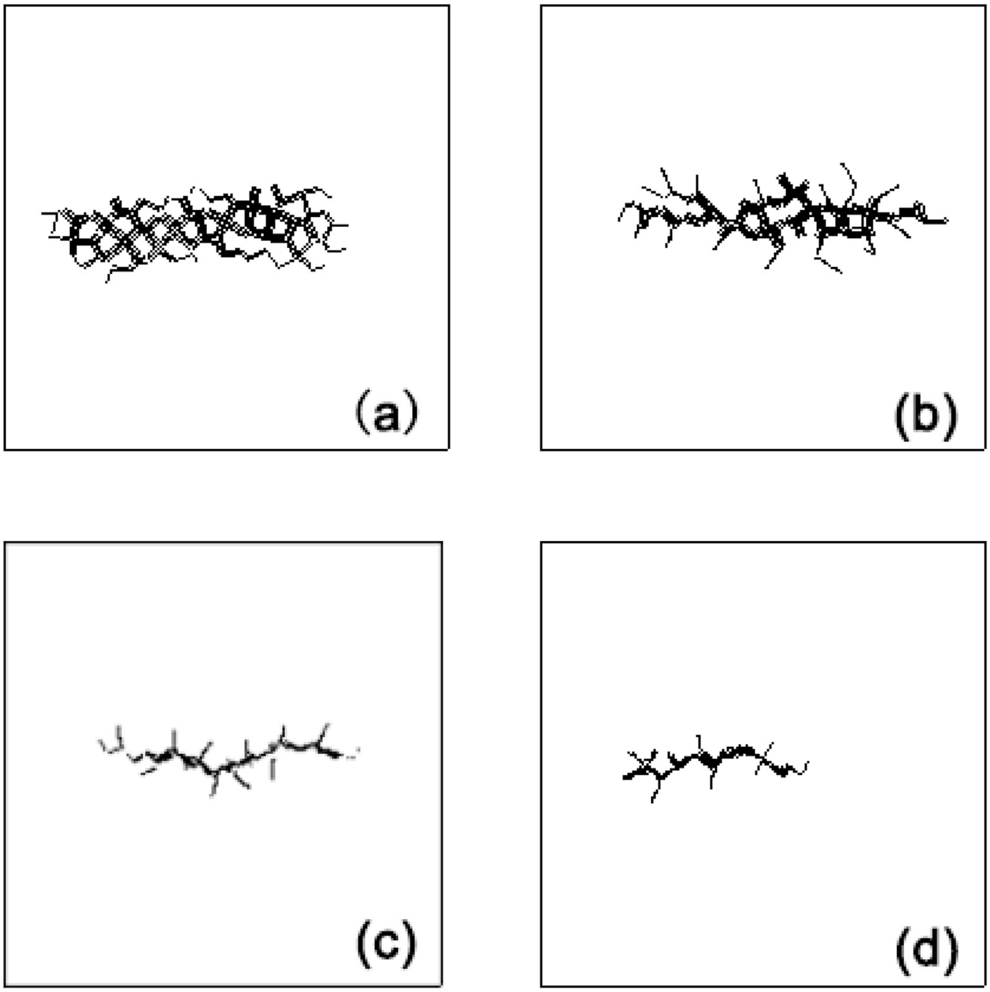

Fig. 11. Distribution of resulting hydraulic fractures in rock masses with randomly oriented joints under different in-situ stresses ($t = 10$ s): (a) $\sigma_y = 8$ MPa; (b) $\sigma_y = 10$ MPa; (c) $\sigma_y = 12$ MPa; (d) $\sigma_y = 14$ MPa.

crack opening increases with an increase of K and the breakdown pressure changes little and is maintains at ~22 MPa.

5.1.2. *Stress magnitude*

Cases 5–8 have a fixed stress ratio ($K = 2$), but the vertical stress σ_y is varied from 8 to 14 MPa. Fig. 11 shows that with a gradual increase of principal stress, the number of hydraulic fractures decreases. Thus, it is difficult for the HF to form under conditions of high in-situ stress, and the fracture extension is correspondingly more difficult. High in situ stress reflects increasingly buried condition for the rock mass, where the initial cracks in rock masses are closed and the rock mass has a low permeability. The form of the HF needs to overcome the effect of this high in-situ stress. Hence, under the same stress ratio conditions, the smaller in situ stress allows the rock mass to be more easily fractured, and the speed of crack propagation will be faster.

5.2. *Water injection rate*

To study the influence of water injection rate on the fracture propagation characteristics of HFs, four representative values of water injection rate are applied. The distribution of hydraulic fractures in the rock mass with random joints under different water injection rates is shown in Fig. 12. The maximum crack opening and breakdown pressure for each solution are shown in Fig. 13.

Apparent from Figs. 12 and 13 is that: with the gradual increase of water injection rate, the distribution of hydraulic fractures expands, and the maximum crack opening is also increased. Apparent from Fig. 13, with an increase in the injection rate, the breakdown pressure gradually increases. The distribution and quantity of resulting fractures and the water injection rate are positively correlated, and the maximum crack opening and the water injection rate are also positively correlated. In addition, the water injection rate and the breakdown pressure of rock mass with random joints are positively correlated.

5.3. *Fluid viscosity*

Viscosity is another important component defining fluid properties and is typically in the range 0.001–1 Pa s, for water-based fluids. According to their viscosity, fluids can be divided into low-viscous, medium-viscous and highly viscous types. The characteristics of the resulting HF propagation in random jointed rock masses with four different fluid viscosities was explored, as shown in Fig. 14. The maximum crack opening and breakdown pressure of each solution is shown in Fig. 15.

Apparent from Figs. 14 and 15 is that with a gradual increase in fluid viscosity, the volume of the stimulated zone around the hydraulic fracture is reduced, but the values of maximum crack opening and breakdown pressure both increase. Thus, the increase of fluid viscosity will weaken HF extension in random jointed rock masses. In other words, the distribution and quantity of fractures and the fluid viscosity are negatively correlated, but the maximum crack opening and the fluid viscosity are positively correlated. In addition, the fluid viscosity and the breakdown pressure of random jointed rock masses are also positively correlated.

As fluid pressure in the hole increases, the fluid will enter the borehole wall, due to th presence of multiple pores and fracture surfaces.

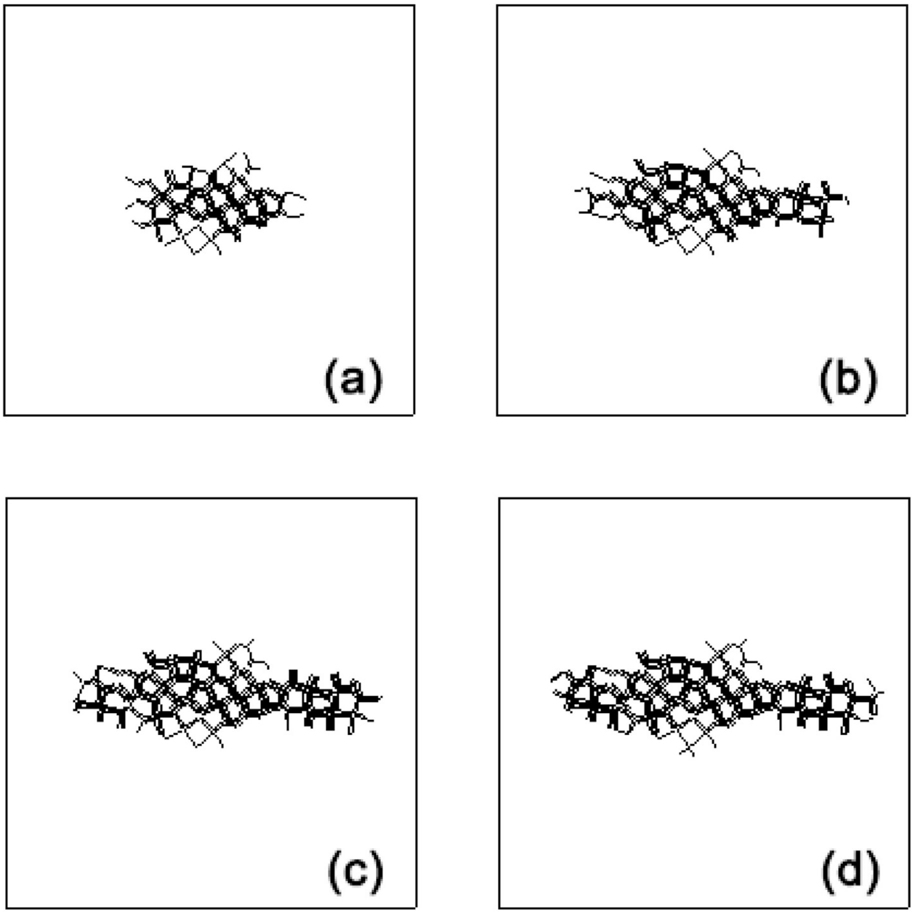

Fig. 12. Distribution of resulting hydraulic fractures in rock masses with random joints under different water injection rates ($t = 10$ s): (a) $Q_0 = 1 \times 10^{-4}$ m^2/s; (b) $Q_0 = 2 \times 10^{-4}$ m^2/s; (c) $Q_0 = 3 \times 10^{-4}$ m^2/s; (d) $Q_0 = 4 \times 10^{-4}$ m^2/s.

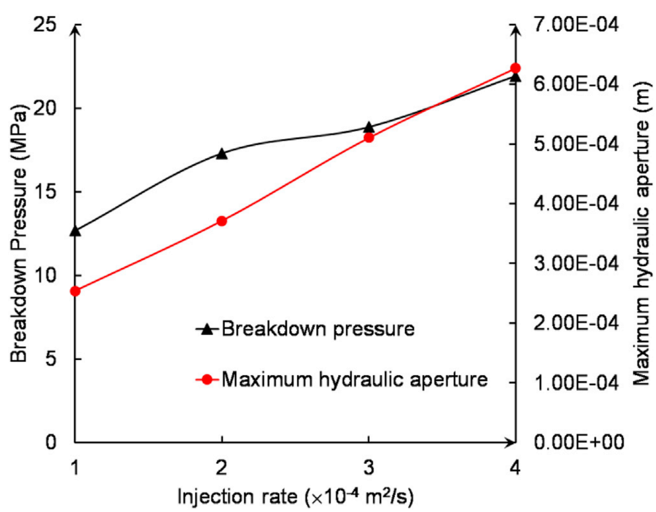

Fig. 13. The effect of water injection rate on breakdown pressure and maximum crack opening.

When fluid viscosity is low, it penetrates readily. This increase in pore pressure reduces the effective stress and the breakdown pressure reduces accordingly - more likely producing cracks. Therefore, under the same conditions, the crack propagation radius for the low viscosity fluid will be larger. Shimizu et al. (2011) report an HF study in intact rock for both low and high viscosity fluids. They show that when the low viscosity fluid is used in the numerical simulation of hydraulic fracturing, cracks form rapidly and the fluid can readily penetrate into the cracks; to the converse, when high viscosity fluid is used, the fluid slowly infiltrates into the cracks, which are mainly concentrated near the borehole wall and the scope of fluid flow is small. These analyses are consistent with these prior observations.

6. Conclusions

In this paper, four typical rock mass models—twin orthogonal joint sets, staggered joint sets, twin diagonal joint sets, and randomly oriented polygonal joint sets—are established to simulate hydraulic fracturing in jointed models based on DEM. The effect of natural existing fractures on fluid-driven hydraulic fracturing is investigated by analyzing the variation of stress ratio, stress magnitude, injection rate, and fluid viscosity. Based on the numerical results, the following conclusions are made:

(1) Numerical simulations have been carried out with UDEC to simulate fluid injection in a preexisting fracture with zero toughness. The numerical predictions for pressure and width at the well have been compared with the analytical first order approximation of the zero-toughness solution (FMO). Also, pressure and width along the fracture have been compared to the FMO solution. The reported UDEC results for fracture growth show an excellent match with the FMO solution. Fluid pressure at the well predicted by UDEC matches well with the FMO solution. The UDEC results for width at the well are bounded by the FMO solution.
(2) Maximum principal stress plays an important role in the process of HF extension. The crack extension directions are always along the maximum principal stress direction in the four kinds of joint rock mass explored here. The presence and texture of joints can produce induced effects on the propagation of the crack, in the process of the extension of HF, continuous high-pressure fluid

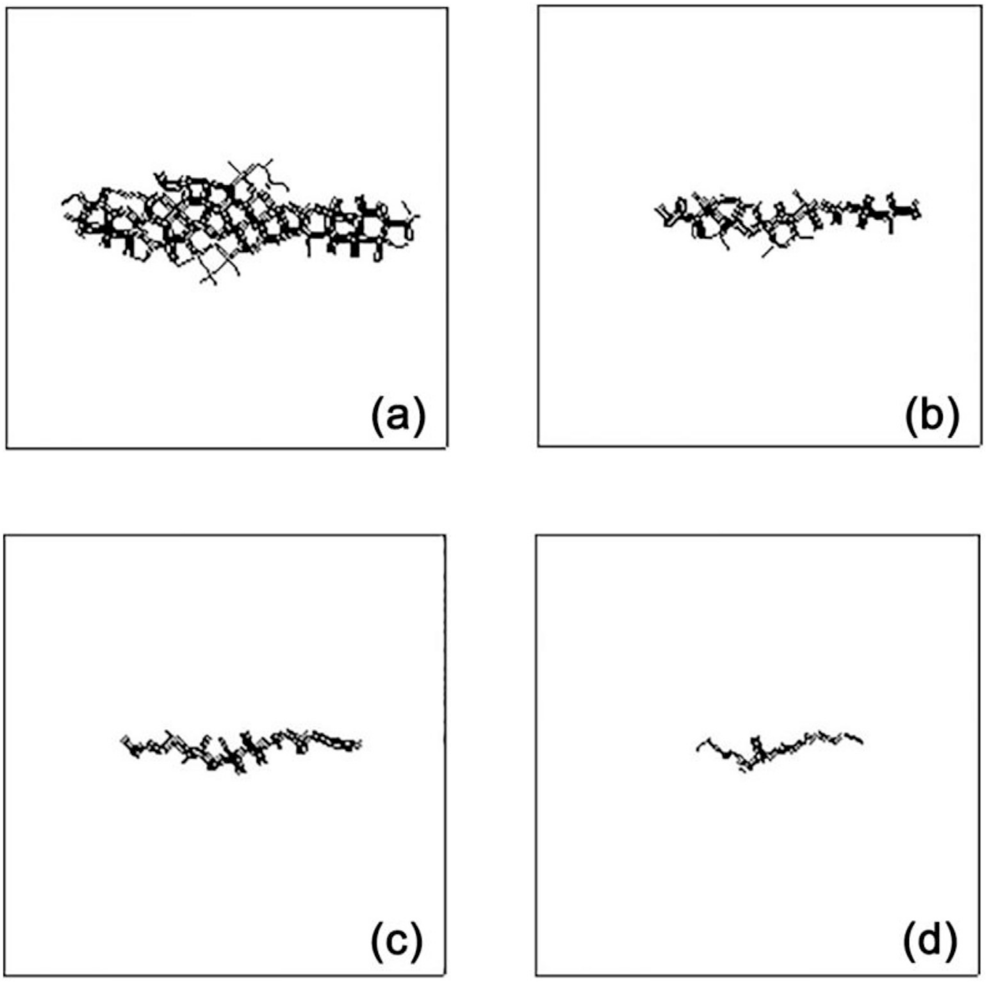

Fig. 14. Distribution of fractures in rock masses with random joints under different values of fluid viscosity ($t = 10$ s): (a) $\mu = 0.001$ Pa s; (b) $\mu = 0.01$ Pa s; (c) $\mu = 0.1$ Pa s; (d) $\mu = 1$ Pa s.

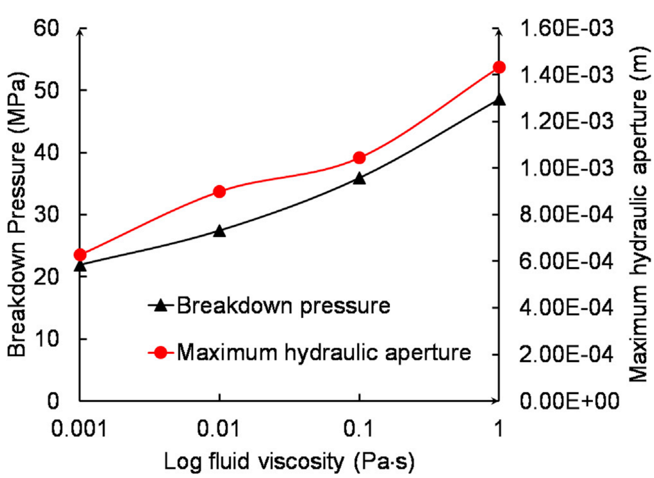

Fig. 15. The effect of fluid viscosity on breakdown pressure and maximum crack opening.

injection will drive the extension of cracks along the joint plane. The greater the initial integrity of rock masses, the higher the breakdown pressure.

(3) For different in-situ stress conditions of a random jointed rock mass, the HF numerical simulation results are: when the difference in in-situ stresses is sufficiently large, the HF will mainly extend parallel to the direction of the maximum principal stress; when the difference is small, radial hydraulic fractures will extend uniformly outward. Under the same conditions, if the difference in in-situ stresses is greater, a discrete HF is more likely to occur. Moreover, the higher in-situ stress conditions make HF more difficultly to form and extend.

(4) For different water injection rates into a random jointed rock mass, the numerical simulation results are: under the same conditions, an increase in water injection rate more easily fractures the rock mass, and the HF propagation radius will correspondingly increase. Meanwhile, a higher breakdown pressure and wider hydraulic aperture will result. With an increase in fluid viscosity, the longitudinal and transverse crack extended ranges are accordingly decreased. By using a low viscosity fluid, crack formation is easier, and the fluid will infiltrate more quickly into the crack. However, when the fluid viscosity is high, the process of fluid permeating through the cracks will be more difficult. Thus, the breakdown pressure and the maximum crack opening are positively correlated with fluid viscosity.

Acknowledgments

The work reported in this paper is financially supported by National Key Basic Research Program of China (973 Program) under Grant No. 2015CB057905 and the National Natural Science Foundation of China (NSFC) under the Contract No. 41504016, 41772305.

References

Adachi, J.I., Detournay, E., 2002. Self-similar solution of a plane-strain fracture driven by a power-law fluid. Int. J. Numer. Anal. Meth. GeoMech. 26, 579–604. https://doi.org/10.1002/nag.213.

Adachi, J., Siebrits, E., Peirce, A., Desroches, J., 2007. Computer simulation of hydraulic fractures. Int. J. Rock Mech. Min. Sci. 44, 739–757. https://doi.org/10.1016/j.ijrmms.2006.11.006.

Al-Busaidi, A., Hazzard, J.F., Young, R.P., 2005. Distinct element modeling of hydraulically fractured Lac du Bonnet granite. J. Geophys. Res. B Solid Earth 110, 1–14. https://doi.org/10.1029/2004JB003297.

Choi, S.O., 2012. Interpretation of shut-in pressure in hydrofracturing pressure-time records using numerical modeling. Int. J. Rock Mech. Min. Sci. 50, 29–37. https://doi.org/10.1016/j.ijrmms.2011.12.001.

Damjanac, B., Cundall, P., 2016. Application of distinct element methods to simulation of hydraulic fracturing in naturally fractured reservoirs. Comput. Geotech. 71, 283–294. https://doi.org/10.1016/j.compgeo.2015.06.007.

Detournay, E., 2004. Propagation regimes of fluid-driven fractures in impermeable rocks. Int. J. GeoMech. 4, 35–45. https://doi.org/10.1061/(ASCE)1532-3641(2004)4:1(35).

Grasselli, G., Lisjak, A., Mahabadi, O.K., Tatone, B.S.A., 2015. Influence of pre-existing discontinuities and bedding planes on hydraulic fracturing initiation. Eur. J. Environ. Civ. Eng 19, 580–597. https://doi.org/10.1080/19648189.2014.906367.

Han, Y., Damjanac, B., Nagel, N., 2012. A microscopic numerical system for modeling interaction between natural fractures and hydraulic fracturing. In: Proceedings of the 46th US Rock Mechanics/Geomechanics Symposium. Chicago, IL. ARMA-2012-238.

Harper, T.R., Last, N.C., 1990. Response of fractured rock subject to fluid injection part II: characteristic behavior. Tectonophysics 172 (1–2), 33–51.

Itasca Consulting Group Inc, 2015. UDEC-universal Distinct Element Code. Ver. 6.0 User's Manual. ICG, Minneapolis.

Lemos, J., Lorig, L.J., 1990. Hydromechanical Modelling of Jointed Rock Masses Using the Distinct Element Method, Mechanics of Jointed and Faulted Rock. Balkema, Rotterdam.

McLennan, J., Tran, D., Zhao, N., Thakur, S., Deo, M., Gil, I., Damjanac, B., 2010. Modeling fluid invasion and hydraulic fracture propagation in naturally fractured rock : a three-dimensional approach. In: SPE Int. Symp. Exhib. Form. Damage Control, p. 13. https://doi.org/10.2118/127888-MS.

Papanastasiou, P.C., 1997. A coupled elastoplastic hydraulic fracturing model. Int. J. rock Mech. Min. Sci. Geomech. Abstr 34 (431). https://doi.org/10.1016/S1365-1609(97)00132-9.

Potyondy, D.O., Cundall, P.A., 2004. A bonded-particle model for rock. Int. J. Rock Mech. Min. Sci. https://doi.org/10.1016/j.ijrmms.2004.09.011.

Riahi, A., Damjanac, B., 2013. Numerical study of the interaction between injection and the discrete fracture network in enhanced geothermal reservoirs. In: Proceedings of the 47th US Rock Mechanics/Geomechanics Symposium. San Francisco, CA. ARMA-2013-333.

Settari, A., Cleary, M.P., 1986. Development and testing of a pseudo-three-dimensional model of hydraulic fracture geometry. SPE Prod. Eng. 1, 449–466. https://doi.org/10.2118/10505-PA.

Shimizu, H., 2010. Distinct Element Modelling for Fundamental Rock Fracturing and Application to Hydraulic Fracturing. Kyoto University.

Shimizu, H., Murata, S., Ishida, T., 2011. The distinct element analysis for hydraulic fracturing in hard rock considering fluid viscosity and particle size distribution. Int. J. Rock Mech. Min. Sci. 48, 712–727. https://doi.org/10.1016/j.ijrmms.2011.04.013.

Veatch Jr., R.V., 1983. Overview of current hydraulic fracturing design and treatment technology. Part 1. J. Petrol. Technol. 35 (4).

Vychytil, J., Horii, H., 1998. Micromechanics-based continuum model for hydraulic fracturing of jointed rock masses during HDR stimulation. Mech. Mater. 28, 123–135. https://doi.org/10.1016/S0167-6636(97)00061-6.

Wang, J.G., Zhang, Y., Liu, J.S., Zhang, B.Y., 2010. Numerical simulation of geofluid focusing and penetration due to hydraulic fracture. J. Geochem. Explor. 106, 211–218. https://doi.org/10.1016/j.gexplo.2009.11.009.

Wang, T., Hu, W., Elsworth, D., Zhou, W., Zhou, W., Zhao, X., Zhao, L., 2017. The effect of natural fractures on hydraulic fracturing propagation in coal seams. J. Petrol. Sci. Eng. 150, 180–190. https://doi.org/10.1016/j.petrol.2016.12.009.

Wang, T., Zhou, W., Chen, J., Xiao, X., Li, Y., Zhao, X., 2014. Simulation of hydraulic fracturing using particle flow method and application in a coal mine. Int. J. Coal Geol. 121, 1–13. https://doi.org/10.1016/j.coal.2013.10.012.

Warpinski, N.R., Teufel, L.W., 1987. Influence of geologic discontinuities on hydraulic fracture propagation (includes associated papers 17011 and 17074). J. Petrol. Technol. 39, 209–220. https://doi.org/10.2118/13224-PA.

Wang, Z.-Q., Detournay, E., 2018. The tip region of a near-surface hydraulic fracture. J. Appl. Mech. https://doi:10.1115/1.4039044.

Yuan, B., Moghanloo, G.R., Zheng, D., 2017a. A novel integrated production analysis workflow for evaluation, optimization and predication in shale plays. Int. J. Coal Geol. 180, 18–28.

Yuan, B., Rouzbeh, G., Moghanloo, R., 2017b. Analytical Modeling Improved Well Performance by Nanofluid Pre-flush. Fuel 202, 380–394. https://doi.org/10.1016/j.fuel.2017.04.004.

Yuan, B., Moghanloo, R., Wang, W., 2018. Using nanofluids to control fines migration for oil recovery: nanofluids co-injection or nanofluids pre-flush? – A comprehensive answer. Fuel 215, 474–483. https://doi.org/10.1016/j.fuel.2017.11.088.

Zhang, G.M., Liu, H., Zhang, J., Wu, H.A., Wang, X.X., 2010. Three-dimensional finite element simulation and parametric study for horizontal well hydraulic fracture. J. Petrol. Sci. Eng. 72, 310–317. https://doi.org/10.1016/j.petrol.2010.03.032.